Unlocking synergy in bimetallic catalysts by core–shell design

Jessi E. S. van der Hoeven[1,2], Jelena Jelic[3], Liselotte A. Olthof[1,2], Giorgio Totarella[1],
Relinde J. A. van Dijk-Moes[2], Jean-Marc Krafft[4], Catherine Louis[4], Felix Studt[3,5],
Alfons van Blaaderen[2✉] and Petra E. de Jongh[1✉]

Extending the toolbox from mono- to bimetallic catalysts is key in realizing efficient chemical processes[1]. Traditionally, the performance of bimetallic catalysts featuring one active and one selective metal is optimized by varying the metal composition[1-3], often resulting in a compromise between the catalytic properties of the two metals[4-6]. Here we show that by designing the atomic distribution of bimetallic Au–Pd nanocatalysts, we obtain a synergistic catalytic performance in the industrially relevant selective hydrogenation of butadiene. Our single-crystalline Au-core Pd-shell nanorods were up to 50 times more active than their alloyed and monometallic counterparts, while retaining high selectivity. We find a shell-thickness-dependent catalytic activity, indicating that not only the nature of the surface but also several subsurface layers play a crucial role in the catalytic performance, and rationalize this finding using density functional theory calculations. Our results open up an alternative avenue for the structural design of bimetallic catalysts.

Synergy arises when two catalytically active metals are combined such that the catalytic performance exceeds that of the monometallic counterparts[1]. This makes bimetallics an interesting class of materials for catalysing a variety of chemical processes ranging from selective hydrogenation[1,5,7] to oxidation[2,4,8] and electrochemical reactions[9-11]. The main focus has been on alloyed nanoparticles, as they are easily accessible with standard catalyst preparation methods and allow facile tuning of their catalytic properties via the average metal composition. However, the arrangement in which the atoms are assembled is also crucial; gas induced and thermally induced metal redistribution can have a large impact on the catalytic performance[12,13]. Thanks to recent advances in material science, it is now possible to synthesize bimetallic nanoparticles with precisely defined atomic arrangements, such as single-atom alloys[14,15], intermetallic structures[16] and core–shell materials[17,18]. Yet, only a limited number of studies systematically link the metal distribution to the performance of bimetallic catalysts[12,13]. In particular, the catalytic behaviour of core–shell nanoparticles is largely unexplored, despite successful demonstrations of core–shell catalysts in electrocatalysis, where changes in the electronic properties of the shell atoms induced by the underlying core resulted in enhanced catalytic performances[9-11,19].

Here, by employing colloid synthesis[18,20], we prepared a well-defined Au–Pd model system with a precisely tunable atomic structure allowing a direct correlation between the metal distribution, composition and crystal structure, and catalytic performance. Specifically, we test these catalysts in the selective hydrogenation of 1,3-butadiene, which is a crucial reaction in purifying alkene feedstock for the polymer industry. The challenge is to selectively convert polyolefins, without hydrogenation of mono-olefins, which are in large excess. Pd-based materials are active hydrogenation catalysts as hydrogen is easily dissociated on the Pd surface[21]. At low conversions, Pd catalysts can be quite selective[22]. However, near full conversion, the hydrogenation of mono-olefins becomes increasingly important[23]. By combining Pd with a less active, more selective metal like Au, or poisoning it with sulfur, such over-hydrogenation can be suppressed[1,24-27], but not without compromising activity compared to pure Pd (refs. [5,28]).

In this work, we designed model catalysts consisting of Au-core Pd-shell nanorods coated with a protective mesoporous silica shell (Au@Pd@SiO$_2$ NRs), as schematically shown in Fig. 1a. The AuNRs have a single-crystalline face centred cubic (fcc) structure with {110} and {100} surface facets exposed along the length of the rod[29]. The Pd-shell thickness was varied by changing the Pd precursor to obtain NRs with different shell thicknesses (Fig. 1b and Supplementary Table 1). This resulted in Au@Pd@SiO$_2$ NRs with an atomic Pd fraction $X_{Pd}=0.04, 0.08, 0.21$ and 0.32 corresponding to the number of Pd layers, $N_{Pd}=1, 2, 5$ and 6 Pd layers, respectively. We ensured that the different batches of Au@Pd@SiO$_2$ had a similar volume by performing the metal overgrowth for the low Pd content samples directly on as-synthesized Au@SiO$_2$ NRs and for the highest Pd content NRs on smaller, pre-etched Au cores.

The high-angle annular dark-field scanning electron microscopy images in Fig. 1c–f confirm that the NRs were monodisperse in size and shape, and were ~70 nm and 20 nm in length and diameter, respectively (Supplementary Table 2). The energy-dispersive X-ray spectroscopy (EDX) maps, depicting a two-dimensional projection of the elemental distribution (Au, Pd and Si are shown in red, green and blue, respectively), clearly reveal the Au-core Pd-shell structure and show that the rods were homogeneous in composition, meaning that every particle had a similar Pd content. Note that there is a slightly higher Pd content at the NR tips, which can be homogenized via mild thermal treatment at 250 °C in H$_2$, resulting in a smooth, epitaxial Pd-on-Au shell (Supplementary Fig. 1). The Si signal in the EDX maps shows that each NR was encapsulated with an 18-nm-thick mesoporous silica shell. This shell protected the particles from deformation and sintering in the subsequent catalytic testing, whereas the mesopores

[1]Materials Chemistry and Catalysis, Debye Institute for Nanomaterials Science, Utrecht University, Utrecht, The Netherlands. [2]Soft Condensed Matter, Debye Institute for Nanomaterials Science, Utrecht University, Utrecht, The Netherlands. [3]Institute of Catalysis Research and Technology, Karlsruhe Institute of Technology, Eggenstein-Leopoldshafen, Germany. [4]Laboratoire de Réactivité de Surface, Sorbonne Université, CNRS, Paris, France. [5]Institute for Chemical Technology and Polymer Chemistry, Karlsruhe Institute of Technology, Karlsruhe, Germany. ✉e-mail: A.vanBlaaderen@uu.nl; P.E.deJongh@uu.nl
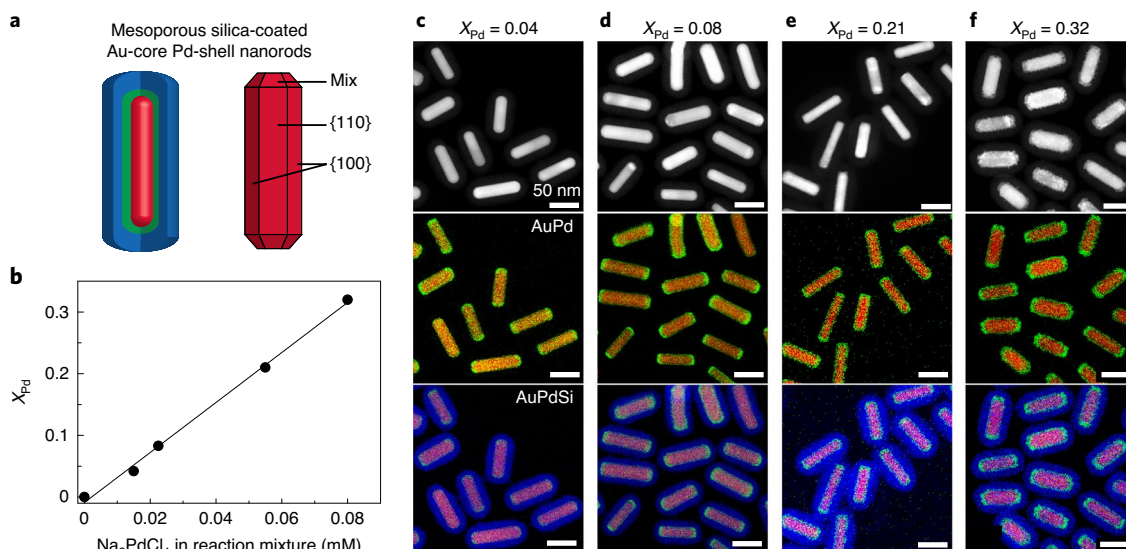
Fig. 1 | Our model system of monodisperse Au@Pd@SiO₂ NRs with controlled Pd content and shell thickness. a, Schematic representation of the Au@Pd@SiO₂ NRs and their surface structure. **b**, Atomic Pd fraction as a function of the Pd-precursor (Na₂PdCl₄) concentration present in the synthesis mixture. **c–f**, High-angle annular dark-field scanning transmission electron microscopy and EDX maps showing the structure and composition of Au@Pd@SiO₂ NRs with $X_{Pd} = 0.04$ (**c**), 0.08 (**d**), 0.21 (**e**) and 0.32 (**f**). In the EDX maps, Au, Pd and Si are presented in red, green and blue, respectively.

ensured mass transport to the metal surface. To render Au@Pd@SiO₂ NRs suitable for gas phase catalysis, the organic template and ligand molecules were removed from the mesopores by washing with acidified ethanol (Supplementary Fig. 2) followed by deposition of the NRs on a commercial silica support (Supplementary Fig. 3). The final metal loading in the catalyst bed was 0.02 wt%.

We tested the catalyst performance of the Au@Pd@SiO₂ NRs in the selective hydrogenation of butadiene to butene in the presence of an excess of propene. While keeping the metal composition of the NRs fixed at $X_{Pd} = 0.08$ ($N_{Pd} = 2$), we studied the effect of the metal distribution on the catalyst performance. Upon increasing the pretreatment temperature, the metal structure of the bimetallic NRs changed from core–shell to fully alloyed, as evident from the EDX maps reported in Fig. 2a, with intermediate partially alloyed structures such as the one at 350 °C (Supplementary Figs. 4 and 5 for quantification of the alloying process). Notably, the NRs exhibited an excellent thermal stability, enabling full retention of the particle shape while changing the atomic distribution within the nanoparticles. In Fig. 2b, we show the catalytic activity of the differently pretreated Au@Pd@SiO₂ NRs at a reaction temperature of 60 °C. The catalytic activity is given as a turnover frequency (TOF), which is expressed as the number of butadiene molecules converted per second per metal surface atom. The TOFs of the core–shell structured Au@Pd@SiO₂ NRs (pretreatment temperature, $T_{pre} = 250$–300 °C) were up to 32 times higher than the partially and fully alloyed ($T_{pre} = 400$–450 °C) AuPd@SiO₂ NRs, which can be explained by the diffusion of less-active Au atoms to the NR surface, leading to a change in the nature of the active site and a strong increase in apparent activation energy from 43 to 75 kJ mol⁻¹ (Supplementary Fig. 6 and Supplementary Table 3). Furthermore, the butadiene conversion versus temperature curves (Fig. 2c) show that the core–shell structured NRs were already active at room temperature, even though the metal loading was as low as 0.02 wt% and the particle size relatively large. Additionally, the core–shell NRs exhibited a high selectivity (Fig. 2b and Supplementary Fig. 7) and highly reproducible catalytic performance (Supplementary Fig. 8). Herein, the selectivity was defined as the number of hydrogen molecules used for the conversion of butadiene to butene divided by the total number of consumed hydrogen molecules. In Fig. 2b, we deliberately show

the selectivity at high butadiene conversion (98%), as maintaining high selectivity at low butadiene concentrations is most challenging. Figure 2d displays the selectivity of the differently structured Au@Pd@SiO₂ NRs over the full range of butadiene conversions, showing that the selectivity was larger than 75% for all samples and highest for the alloyed catalysts.

As the core–shell structure exhibited a superior activity while retaining high selectivity, we further investigated the core–shell structures and studied the influence of the shell thickness on the catalytic behaviour. Herein, NRs with 1, 2, 5 and 6 Pd-shell layers and $X_{Pd} = 0.04$, 0.08, 0.21 and 0.32, respectively, were used and compared to a Au and Pd reference catalyst. As it was not feasible to synthesize well-defined monometallic Pd rods, we prepared a catalyst consisting of spherical Pd nanoparticles with an average diameter (d) of 6.1 nm on a silica support as a reference (Supplementary Fig. 9). Furthermore, the monometallic Au NRs were not active enough (conversion ≤20%) to compare them to the Au–Pd and Pd catalyst at the same temperature interval (Supplementary Fig. 10). We therefore included the catalytic performance of a Au-on-silica catalyst ($d = 3.2$ nm, 3.6 wt%) from the literature in Fig. 3 for comparison[27]. In Fig. 3 we show that the bimetallic core–shell NRs outperformed the monometallic Au and Pd catalysts and that the catalytic performance was highly sensitive to the Pd-shell thickness. In Fig. 3a, the catalytic activity (expressed as TOF) at a reaction temperature of 45 °C, and the selectivity at high (98%) butadiene conversion are plotted as a function of the atomic Pd fraction (X_{Pd}). All core–shell structures with more than one Pd layer were considerably more active than the monometallic Au and Pd nanoparticles and exhibited very high TOFs. For comparison, the TOF of much smaller, 2–3 nm Au–Pd nanoparticles on silica ($X_{Pd} = 0.05$) tested under the same conditions was 0.001 to 0.1 s⁻¹ at 60 °C (ref. [28]). The high activity of the Au@Pd@SiO₂ catalysts is confirmed by the conversion profiles in Fig. 3b. Interestingly, the activity of the Au@Pd@SiO₂ NRs depended on the shell thickness, where six atomic Pd layers were found to be most active in this specific case. The selectivity was highest for the pure Au and Au@Pd@SiO₂ NRs with $N_{Pd} = 1$ and lowest for the pure Pd sample (Fig. 3c and Supplementary Fig. 11). By plotting the selectivity as a function of conversion, we show that the selectivity dropped to lower values for all catalysts
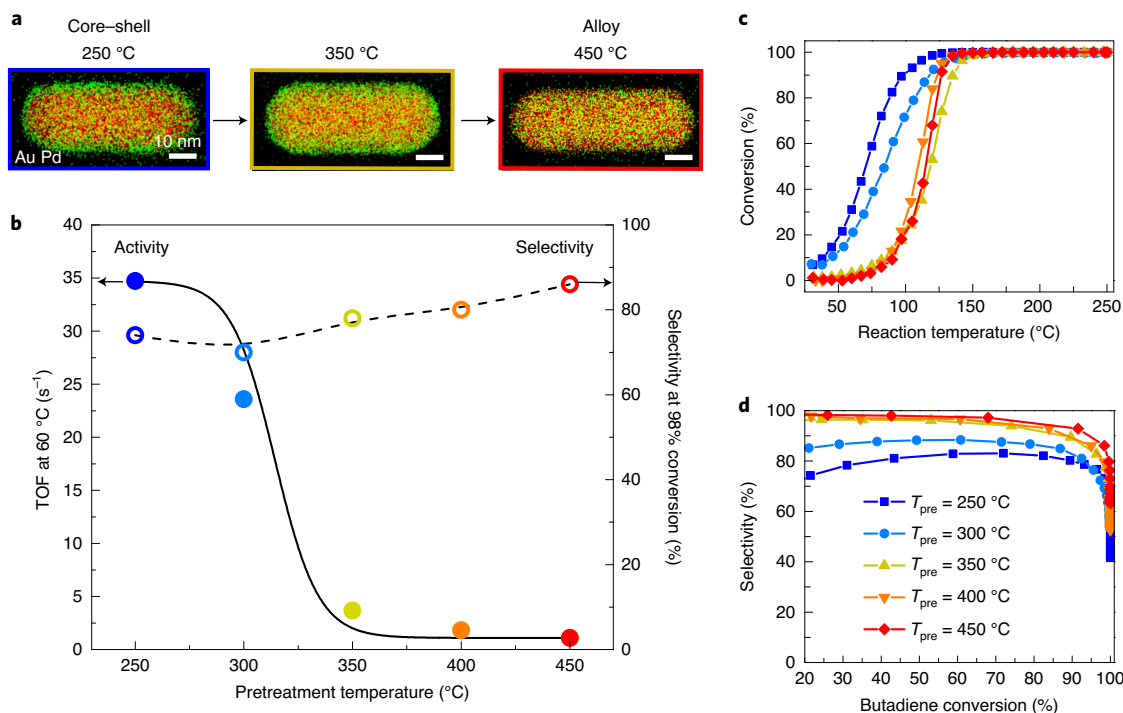
Fig. 2 | Core–shell structured Au–Pd catalysts outperform their alloyed counterparts. a, EDX maps showing core–shell (250 °C), partially alloyed (350 °C) and alloyed (450 °C) Au@Pd@SiO$_2$ NRs with $X_{Pd} = 0.08$ and $N_{Pd} = 2$. **b**, Catalytic activity and selectivity of the differently structured Au@Pd@SiO$_2$ NRs in the selective hydrogenation of butadiene. **c**, Butadiene conversion as a function of reaction temperature of the Au@Pd@SiO$_2$ NRs pretreated at different temperatures (as shown in panel **d**). **d**, Selectivity to butene as a function of the butadiene conversion. For all catalytic tests, 20 mg catalyst with 0.02 wt% metal was used. The reaction mixture consisted of 0.3% butadiene, 30% propene, 20% H$_2$ and an amount of He to balance the flow rate to 50 ml min^{-1}.

at high conversion, yet remained above 80% for the Au@Pd@SiO$_2$ NRs with $N_{Pd} = 1$ and 6. This means that the best combined activity and selectivity for the structures tested in this work was obtained with the core–shell catalyst with $N_{Pd} = 6$, where the TOF was 50 s^{-1} at 45 °C and the selectivity 80% at 98% butadiene conversion.

To understand the catalytic behaviour of the core–shell NRs, we employed density functional theory calculations and studied the effect of the surface facets, Pd-shell thickness and lattice strain on the adsorption energies of butadiene, propene, butene and hydrogen. From our reaction order measurements (Supplementary Fig. 12), it follows that the catalytic activity depends on the butadiene and hydrogen pressure, and is insensitive to the propene pressure. We therefore studied the adsorption energy of butadiene (Fig. 4a) and hydrogen (Supplementary Fig. 13) as a function of the Pd-shell thickness for fcc {100}-, {111}- and {110}-terminated surfaces. These surfaces consist of up to six layers of Pd on Au, as it has been shown experimentally that Pd can grow epitaxially on Au{100} (ref. [30]) and Au{110} (ref. [31]) with thicknesses of six to nine layers. For butadiene, we find a strong dependence on the type of surface facet, with the {110} surface binding butadiene the most strongly. Our results are consistent with previous studies[23,32,33] on Pd and Au–Pd single crystals reporting higher reaction rates at the {110} surface. The {110} surface is therefore likely to dominate the catalytic behaviour of the Au@Pd@SiO$_2$ NRs. Furthermore, since a large part of the NR surface is composed of {110} facets and the activity of Pd catalysts is mostly particle-size independent[23], the high adsorption energies at the {110} facets could, in part, explain the high catalytic activity of our core–shell NRs.

Next, we studied the effect of the shell thickness on the adsorption energies of all reactants on a {110}-terminated surface (Fig. 4b; Supplementary Fig. 14 for the {111} and {100} surfaces).

The ~1 eV difference in binding energy between butadiene and propene/butene explains the high selectivity of Au@Pd@SiO$_2$ NRs as observed experimentally. The increased binding strength of butadiene and hydrogen on the layered Au–Pd structures compared to pure Au explains the increased activity of the core–shell catalysts. The high adsorption energies of the reactants on the core–shell compared to the monometallic catalysts are likely caused by lattice strain stemming from the lattice mismatch between the Au core and Pd overlayer (~4%). This likely cause is supported by the density functional theory calculation results in Fig. 4c, showing the hydrogen and butadiene adsorption energy for pure Pd with a Pd lattice constant and for strained Pd with a Au lattice constant. Lattice-strain-induced changes in reactant binding energies have been observed before, for instance in the oxygen reduction reaction on strained core–shell catalysts[9,11].

We note that the shell-thickness-dependent catalytic activity as measured experimentally does not directly correspond to the density functional theory calculations. The Au@Pd@SiO$_2$ NRs with $N_{Pd} = 1$ and 2 are less active than expected based on the hydrogen and butadiene adsorption energies. Although the EDX analysis revealed an overall core–shell structure after pretreatment at 250 °C (Supplementary Fig. 4), carbon monoxide diffuse reflectance infrared Fourier transform spectroscopy (CO-DRIFTS) revealed slight compositional redistribution at the NR surface for thin Pd shells (Supplementary Fig. 15), likely due to the strong driving force for alloying[31]. The concentration of the resulting Au atoms in the surface layer is known to decrease with increasing shell thickness[31], which is confirmed by the CO-DRIFTS measurements. The shell-thickness-dependent intermixing resulted in more-pure Pd shells for $N_{Pd} = 5$–6 compared to $N_{Pd} = 1$–2. Our density functional theory calculations show that Au impurities in
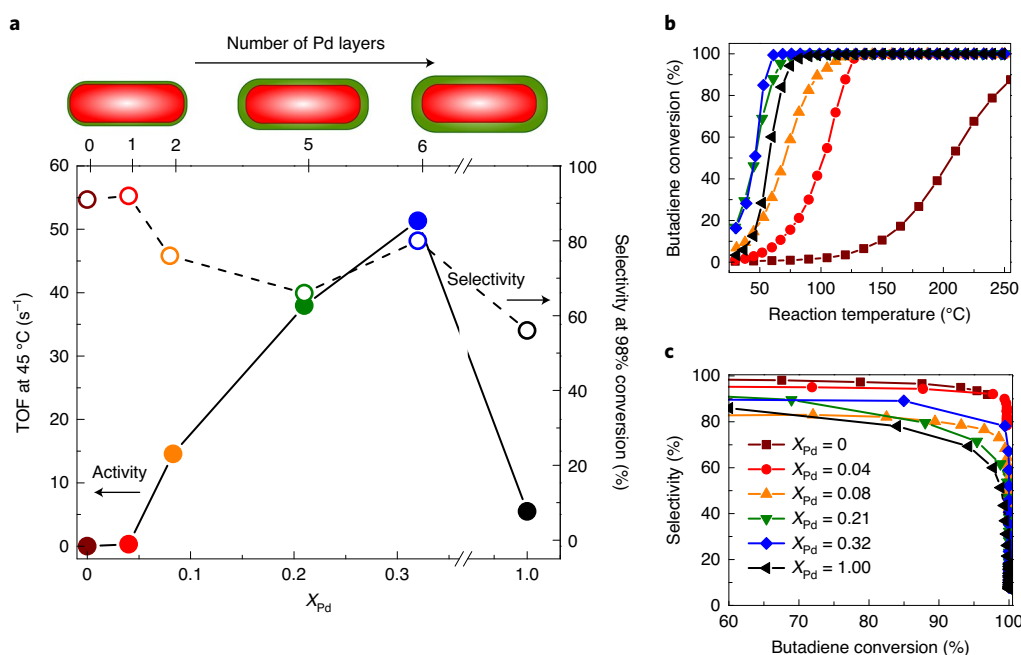
Fig. 3 | The catalytic performance of Au-core Pd-shell catalysts is highly sensitive to the number of shell layers. a, Au@Pd@SiO$_2$ NRs with variable Pd content and shell thickness were used: $X_{Pd}=0.04$, $N_{Pd}=1$ (red); $X_{Pd}=0.08$, $N_{Pd}=2$ (orange); $X_{Pd}=0.21$, $N_{Pd}=5$ (green); $X_{Pd}=0.32$, $N_{Pd}=6$ (blue); and Au@ SiO$_2$ ($X_{Au}=1.0$, brown) and Pd@SiO$_2$ ($X_{Pd}=1.0$, black) reference samples containing spherical 3.0 and 6.1 nm particles, respectively. Activity expressed as TOF (s^{-1}) at 45 °C (left axis) and the selectivity at 98% butadiene conversion (right axis) as a function of the atomic Pd fraction. **b**, Butadiene conversion as a function of the reaction temperature (as shown in panel **c**). **c**, Selectivity to butene as a function of the butadiene conversion. The metal loading for the Au@Pd NRs with $X_{Pd}=0.08$–0.32 and $X_{Pd}=0.04$ was 0.02 wt% and 0.2 wt%, respectively. The metal loading for the Au@SiO$_2$ and Pd@SiO$_2$ reference samples was 3.6 and 0.0065 wt%, respectively.
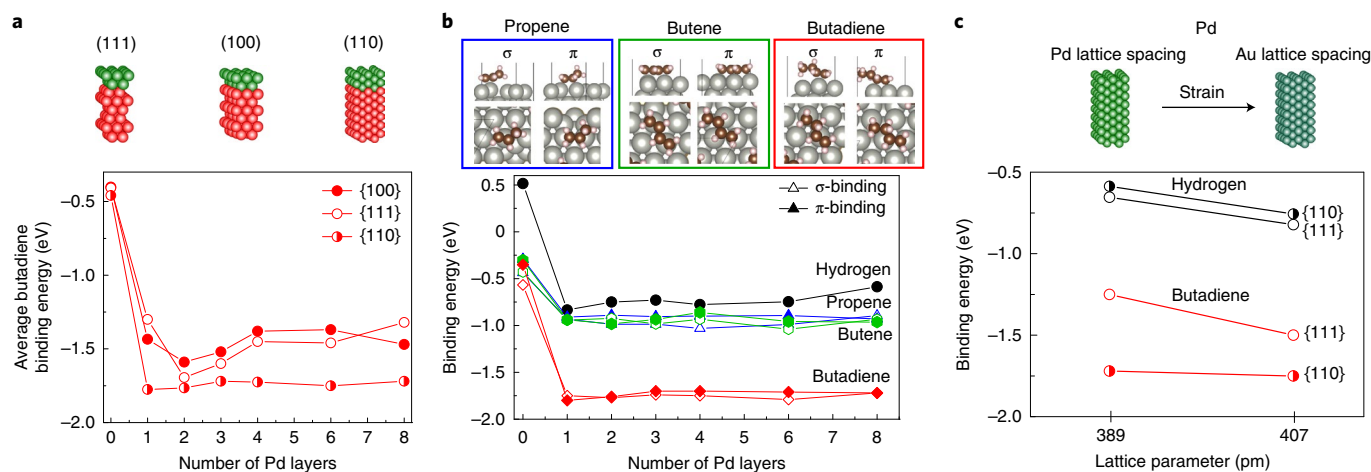
Fig. 4 | Crystallographic orientation of the surface facets, Pd-shell thickness and lattice strain govern the reactant adsorption energies. a, Average adsorption energy of butadiene as a function of the number of Pd layers at a {100}, {111} and {110} surface. **b**, Schematic representation of the σ and π binding modes and plot of the binding energy as a function of the Pd-shell thickness of hydrogen (black), propene (blue), butene (green) and butadiene (red). **c**, Hydrogen and butadiene adsorption on Pd and strained Pd{111} and {110} surfaces with a Pd (389 pm) and Au (407 pm) lattice parameter are given, respectively.

the upper Pd surface layer lower the binding energy of butadiene by 0.6 eV (Supplementary Fig. 16), explaining the lower activity for thin Pd layers. This is further supported by the increase in the pre-exponential factor for $N_{Pd}=1$ to 6 (Supplementary Table 4), indicating an increase of the number of active sites with increasing shell thickness. Finally, we would like to note that increasing the shell thickness above six to nine layers[30,31] would likely lead to loss of

the epitaxial nature of the Pd shell and the formation of separate Pd nanoparticles, and hence would lead to catalytic behaviour similar to that of pure Pd.

Altogether, we have shown that core–shell catalysts are considerably more active than their alloyed counterparts, that their catalytic performance is shell-thickness dependent and that the properties of Au-core Pd-shell catalysts do not resemble those of pure Pd even up

to six atomic Pd-shell layers. Our study highlights the importance of tuning the atomic distribution in bimetallic catalysts, and lays a foundation for the rational design of bimetallic catalysts with optimal synergistic performances.

Online content

References

1. Zhang, L., Zhou, M., Wang, A. & Zhang, T. Selective hydrogenation over supported metal catalysts: from nanoparticles to single atoms. *Chem. Rev.* **120**, 683–733 (2020).
2. Wu, C. H. et al. Bimetallic synergy in cobalt–palladium nanocatalysts for CO oxidation. *Nat. Catal.* **2**, 78–85 (2019).
3. Studt, F. et al. Identification of non-precious metal alloy catalysts for selective hydrogenation of acetylene. *Science* **320**, 1320–1322 (2008).
4. Enache, D. I. et al. Solvent-free oxidation of primary alcohols to aldehydes using Au-Pd/TiO₂ catalysts. *Science* **311**, 362–365 (2006).
5. Hugon, A., Delannoy, L., Krafft, J. M. & Louis, C. Selective hydrogenation of 1,3-butadiene in the presence of an excess of alkenes over supported bimetallic gold palladium catalysts. *J. Phys. Chem. C* **114**, 10823–10835 (2010).
6. Masoud, N., Delannoy, L., Calers, C. & Gallet, J. J. Silica-supported Au–Ag catalysts for the selective hydrogenation of butadiene. *Chem. Cat. Chem.* **9**, 2418–2425 (2017).
7. Lucci, F. R. et al. Selective hydrogenation of 1,3-butadiene on platinum–copper alloys at the single-atom limit. *Nat. Commun.* **6**, 8550 (2015).
8. Wang, G. H. et al. Platinum–cobalt bimetallic nanoparticles in hollow carbon nanospheres for hydrogenolysis of 5-hydroxymethylfurfural. *Nat. Mater.* **13**, 293–300 (2014).
9. Bu, L. et al. Biaxially strained PtPb/Pt core/shell nanoplate boosts oxygen reduction catalysis. *Science* **354**, 1410–1414 (2016).
10. Wang, X. et al. Palladium–platinum core–shell icosahedra with substantially enhanced activity and durability towards oxygen reduction. *Nat. Commun.* **6**, 7594 (2015).
11. Strasser, P. et al. Lattice-strain control of the activity in dealloyed core–shell fuel cell catalysts. *Nat. Chem.* **2**, 454–460 (2010).
12. Zugic, B. et al. Dynamic restructuring drives catalytic activity on nanoporous gold–silver alloy catalysts. *Nat. Mater.* **16**, 558–565 (2016).
13. Ahmadi, M., Behafarid, F., Cui, C., Strasser, P. & Cuenya, B. R. Long-range segregation phenomena in shape-selected bimetallic nanoparticles: chemical state effects. *ACS Nano* **7**, 9195–9204 (2013).
14. Wrasman, C. J. et al. Synthesis of colloidal Pd/Au dilute alloy nanocrystals and their potential for selective catalytic oxidations. *J. Am. Chem. Soc.* **140**, 12930–12939 (2018).
15. Luneau, M. et al. Dilute Pd/Au alloy nanoparticles embedded in colloid-templated porous SiO₂: stable Au-based oxidation catalysts. *Chem. Mater.* **31**, 5759–5768 (2019).
16. Lee, J. D. et al. Tuning the electrocatalytic oxygen reduction reaction activity of Pt-Co nanocrystals by cobalt concentration with atomic-scale understanding. *ACS Appl. Mater. Interfaces* **11**, 26789–26797 (2019).
17. Gilroy, K. D., Ruditskiy, A., Peng, H. C., Qin, D. & Xia, Y. Bimetallic nanocrystals: syntheses, properties, and applications. *Chem. Rev.* **116**, 10414–10472 (2016).
18. Deng, T. S. et al. Oxidative etching and metal overgrowth of gold nanorods within mesoporous silica shells. *Chem. Mater.* **27**, 7196–7230 (2015).
19. Zhang, Y. J. et al. Probing the electronic structure of heterogeneous metal interfaces by transition metal shelled gold nanoparticle-enhanced Raman spectroscopy. *J. Phys. Chem. C* **120**, 20684–20691 (2016).
20. van der Hoeven, J. E. S. et al. *In situ* observation of atomic redistribution in alloying gold–silver nanorods. *ACS Nano* **12**, 8467–8476 (2018).
21. Yu, W. Y., Mullen, G. M. & Mullins, C. B. Hydrogen adsorption and absorption with Pd–Au bimetallic surfaces. *J. Phys. Chem. C* **117**, 19535–19543 (2013).
22. Molnár, A., Sárkány, A. & Varga, M. Hydrogenation of carbon–carbon multiple bonds: chemo-, regio- and stereo-selectivity. *J. Mol. Catal. A Chem.* **173**, 185–221 (2001).
23. Silvestre-Albero, J., Rupprechter, G. & Freund, H. J. From Pd nanoparticles to single crystals: 1,3-butadiene hydrogenation on well-defined model catalysts. *Chem. Commun.* 80–82 (2006).
24. Bachiller-Baeza, B. et al. Detecting the genesis of a high-performance carbon-supported Pd sulfide nanophase and its evolution in the hydrogenation of butadiene. *ACS Catal.* **5**, 5235–5241 (2015).
25. McEwan, L., Juliusa, M., Robertsa, S. & Fletchera, J. C. Q. A review of the use of gold catalysts in selective hydrogenation reactions. *Gold. Bull.* **43**, 298–306 (2010).
26. Hugon, A., Delannoy, L. & Louis, C. Supported gold catalysts for selective hydrogenation of 1,3-butadiene in the presence of an excess of alkenes. *Gold. Bull.* **41**, 127–138 (2008).
27. Masoud, N. et al. Superior stability of Au/SiO₂ compared to Au/TiO₂ catalysts for the selective hydrogenation of butadiene. *ACS Catal.* **7**, 5594–5603 (2017).
28. Kolli, N. E., Delannoy, L. & Louis, C. Bimetallic Au–Pd catalysts for selective hydrogenation of butadiene: influence of the preparation method on catalytic properties. *J. Catal.* **297**, 79–92 (2013).
29. Goris, B. et al. Atomic-scale determination of surface facets in gold nanorods. *Nat. Mater.* **11**, 930–935 (2012).
30. Pinheiro, A., Zei, M., Luo, M. & Ertl, G. The epitaxial growth of Pd electrodeposition on Au(100) studied by LEED and RHEED. *Surf. Sci.* **600**, 641–650 (2006).
31. Dolle, P. et al. Strained Pd films, by epitaxial growth on Au(110), to control catalytic properties. *Surf. Sci.* **518**, 1–13 (2002).
32. Bertolini, J. C. et al. Electronic properties of supported Pd aggregates in relation with their reactivity for 1,3-butadiene hydrogenation. *Catal. Lett.* **6**, 215–223 (1990).
33. Piccolo, L., Piednoir, A. & Bertolini, J. C. Pd-Au single-crystal surfaces: segregation properties and catalytic activity in the selective hydrogenation of 1,3-butadiene. *Surf. Sci.* **592**, 169–181 (2005).

Author contributions

J.E.S.v.d.H. performed the experiments supervised by A.v.B. and P.E.d.J.; J.J. performed the calculations under the supervision of F.S.; L.A.O. synthesized the NRs supervised by J.E.S.v.d.H.; and G.T. assisted in the catalysis experiments. R.J.A.v.D.-M. performed the inductively coupled plasma atomic emission spectroscopy measurements. J.-M.K. and C.L. conducted and interpreted the CO-DRIFTS analysis. J.E.S.v.d.H. and P.E.d.J. wrote the paper with the contributions of all the authors.

Competing interests

The authors declare no competing interests.

Additional information

Supplementary information The online version contains supplementary material available at https://doi.org/10.1038/s41563-021-00996-3.

Correspondence and requests for materials should be addressed to A.v.B. or P.E.d.J.

Peer review information *Nature Materials* thanks the anonymous reviewers for their contribution to the peer review of this work.

Reprints and permissions information is available at www.nature.com/reprints.